 CMES, vol.x, no.x, pp.1-15, 2003

Numerical Computation of Discrete Differential Operators on Non-Uniform Grids

N. Sukumar[1] **and J. E. Bolander**[1]

Abstract: In this paper, we explore the numerical approximation of discrete differential operators on non-uniform grids. The Voronoi cell and the notion of natural neighbors are used to approximate the Laplacian and the gradient operator on irregular grids. The underlying weight measure used in the numerical computations is the *Laplace weight function*, which has been previously adopted in meshless Galerkin methods. We develop a difference approximation for the diffusion operator on irregular grids, and present numerical solutions for the Poisson equation. On regular grids, the discrete Laplacian is shown to reduce to the classical finite difference scheme. Two techniques to compute the nodal (gradient) flux are presented, and benchmark computations in 2-d are performed to demonstrate the accuracy of the schemes. The numerical approximations developed herein are of relevance in the solution of partial differential equations, in methods where local (Laplacian) smoothing is desired, and for applications such as mesh adaptivity in which a posteriori error estimates using stress-based recovery schemes are used.

keyword: meshless methods, natural neighbor, Voronoi diagram, Laplace interpolant, finite volume, irregular lattice, diffusion, supraconvergence

1 Introduction

The numerical computation of difference approximations on non-uniform (unstructured) grids is used for the solution of partial differential equations, as a means for local smoothing, in a posteriori error estimation using stress-based recovery schemes, and during post-processing of secondary (flux) variables in Galerkin methods. Classical finite difference schemes are typically based on regular grids, and hence are restricted to problem domains with regular geometry. Building on prior work due to Jensen (1972), Liszka and Orkisz (1980) proposed a generalized finite difference method (GFDM) on irregular grids. The central issue addressed in Liszka and Orkisz (1980) was the appropriate selection of the computational cell (star-shaped domain) that surrounds a node, so as to yield a well-conditioned discrete system of equations. Baty and Villon (1997) used a least-squares method, whereas Breitkopf, Touzot, and Villon (2000) adopted moving least squares (MLS) approximants [Lancaster and Salkauskas (1981)] to solve elliptic problems on arbitrary irregular grids. Typically, in these approaches, a system of linear equations is solved to obtain the discrete differential operators [Liszka and Orkisz (1980)].

In this paper, we adopt the Voronoi cell and the notion of natural neighbors to study difference approximations for the diffusion and gradient operators on unstructured grids in multi-dimensions. The advantages of the proposed approach over MLS-based schemes are two-fold:

- For irregularly-spaced nodes, the concept of natural neighbors provides a simple means to determine (uniquely) the neighbors for a point. The geometric properties of the Voronoi cell also provide a weight function for each neighbor.
- Natural neighbor-based interpolation is a local approximation that is well-defined at all points in the domain. The computational costs involved in the construction of the interpolant are also minimal since only algebraic calculations (no matrix inversion or numerical integration) are required in the evaluation of the discrete differential operators.

It was recently brought to our attention [Arroyo (2003)] that a discrete theory of exterior calculus [Hirani (2003); Mathieu, Hirani, Leok, and Marsden (2003)] provides a discrete approximation for the Laplace operator that is identical to the one used here. The calculus of differential forms (see Warnick, Selfridge, and Arnold (1997) for an introduction) rests on foundations in algebraic topology and geometric integration theory, and there has been significant progress in computational mathematics and

[1] Department of Civil and Environmental Engineering, One Shields Avenue, University of California, Davis, CA 95616, U.S.A.

physics towards the construction of discrete counterparts of continuum equations of field theories [Hyman and Shashkov (1997); Teixeira and Chew (1999); Hiptmair (2001); Hirani (2003)]; in a recent workshop[2], some of these topics are discussed. In solid mechanics, efforts are also underway to develop discrete formulations [Tonti (2001); Cosmi (2001); Ferretti (2003)].

In Section 2, an introduction to natural neighbors and natural neighbor-based (Sibson and Laplace) interpolants is provided. The computational algorithm for the Laplace interpolant is discussed in Section 2.2. Then, in Section 3.1, we describe the construction of a Voronoi cell-based difference approximation for the diffusion equation. Issues pertaining to consistency and convergence of difference schemes on non-uniform grids are discussed in Section 3.1.1. Numerical examples for the Poisson equation in 1-d and 3-d are presented in Section 3.1.3. Discrete approximations for the gradient operator are described in Section 3.2, and benchmark computations in 2-d are presented in Section 3.2.3. A discussion of the main results from this study, and a few concluding remarks, are given in Section 4.

2 Natural Neighbor-Based Interpolants

With an aim to overcome the need to remesh in moving boundary and large deformation problems, there has been significant interest in the development and application of meshless Galerkin methods [Belytschko, Krongauz, Organ, Fleming, and Krysl (1996)]. For recent overviews on meshless and particle methods, the interested reader can refer to Li and Liu (2002) and Atluri and Shen (2002a). In the early developments of meshless methods, moving least squares approximants [Lancaster and Salkauskas (1981)] were used to construct the trial and test functions. To improve the speed and cost-effectiveness of meshless computations vis-à-vis finite elements, Atluri and Shen (2002b) have recently examined the use of various combinations of trial and test approximations. Towards the goal of a truly meshless method, Atluri and Shen (2002a,b) have developed the meshless local Petrov-Galerkin method in which elements or background cells are not required either for interpolation or for the integration of the weak form. Natural neighbor-based schemes are a promising alternative to MLS-approximations; in natural neighbor-based Galerkin methods [Sukumar (1998); Sukumar, Moran, Semenov, and Belikov (2001)], the Sibson coordinate [Sibson (1980)] and the Laplace interpolant [Christ, Friedberg, and Lee (1982); Belikov, Ivanov, Kontorovich, Korytnik, and Semenov (1997); Hiyoshi and Sugihara (1999)] are adopted. An overview of natural neighbor Galerkin methods with applications in solid and fluid mechanics is presented in Cueto, Sukumar, Calvo, Cegoñino, and Doblaré (2003).

Consider a bounded domain Ω in d-dimensions (d =1–3) that is described by a set $\mathbf{N}$ of M scattered nodes: $\mathbf{N} = \{n_1, n_2, \ldots, n_M\}$. The Voronoi diagram [Aurenhammer (1996)] $V(\mathbf{N})$ of the set $\mathbf{N}$ is a sub-division of the domain into regions $V(n_I)$, such that any point in $V(n_I)$ is closer to node n_I than to any other node $n_J \in N$ ($J \neq I$). The region $V(n_I)$ is the first-order Voronoi cell for a node n_I within the convex hull; $V(n_I)$ is a convex polygon (polyhedron) in $\mathbf{R}^2$ ($\mathbf{R}^3$):

$$V(n_I) = \{\mathbf{x} \in \mathbf{R}^d : d(\mathbf{x}, \mathbf{x}_I) < d(\mathbf{x}, \mathbf{x}_J)\ \forall J \neq I\}, \quad (1)$$

where $d(\cdot,\cdot)$ denotes the Euclidean distance.

The dual of the Voronoi diagram is the Delaunay tessellation, which is constructed by connecting nodes that have a common (d–1)-dimensional Voronoi facet. In Fig. 1a, the Voronoi diagram and the Delaunay triangulation are shown for a nodal set consisting of seven nodes ($M = 7$). The Voronoi vertex and edge are also indicated in Fig. 1a. A noteworthy property of Delaunay triangles is the *empty circumcircle criterion*—if $DT(n_J, n_K, n_L)$ is any Delaunay triangle of the nodal set $\mathbf{N}$, then the circumcircle of DT contains no other nodes of $\mathbf{N}$. In Fig. 1b, the Delaunay circumcircles for three triangles are shown. Consider the introduction of a point p with coordinate $\mathbf{x} \in \mathbf{R}^2$ into the domain Ω (Fig. 1b). The Voronoi diagram $V(n_1, n_2, \ldots, n_M, p)$ or equivalently the Delaunay triangulation $DT(n_1, n_2, \ldots, n_M, p)$ for the M nodes and the point p is constructed. Now, if the Voronoi cell for p and n_I have a common facet (line segment in $\mathbf{R}^2$ and a polygon in $\mathbf{R}^3$), then the node n_I is said to be a *natural neighbor* of the point p [Sibson (1980)]. The Voronoi cell for point p and its natural neighbors are shown in Fig. 1c.

The Sibson coordinate is based on the first- and second-order Voronoi diagram [Aurenhammer (1996)] and is de-

[2] Workshop on Mimetic Discretizations of Continuum Mechanics; URL: `http://www.sci.sdsu.edu/compscims/MIMETIC`

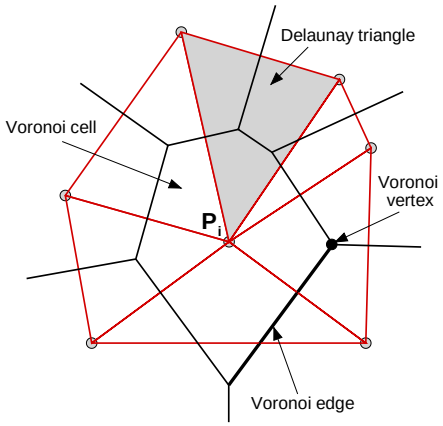

(a)

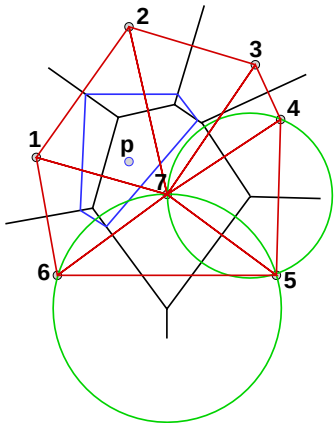

(b)

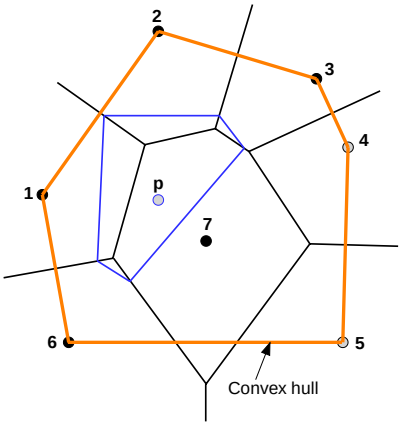

(c)

Figure 1 : Geometric constructs. (a) Voronoi diagram and Delaunay triangulation; (b) Delaunay circumcircles; and (c) Natural neighbors (filled circles) of point p.

fined by the ratio of area measures in 2-d [Sibson (1980)]:

$$\phi_I(\mathbf{x}) = \frac{A_I(\mathbf{x})}{A(\mathbf{x})}, \quad A(\mathbf{x}) = \sum_{J=1}^{n} A_J(\mathbf{x}), \tag{2}$$

where $A(\mathbf{x})$ is the area of the first-order Voronoi cell of p and $A_I(\mathbf{x})$ is the area of overlap between the first-order Voronoi cells of p and node I. In Fig. 2a, the areas $A_1(\mathbf{x})$ (node 1) and $A(\mathbf{x})$ are shown.

The Laplace interpolant was first proposed in Christ, Friedberg, and Lee (1982), with its recent re-discovery in two distinct research groups [Belikov, Ivanov, Kontorovich, Korytnik, and Semenov (1997); Hiyoshi and Sugihara (1999)]. In Belikov, Ivanov, Kontorovich, Korytnik, and Semenov (1997), the new natural neighbor-based interpolant was referred to as the non-Sibsonian interpolant, whereas Hiyoshi and Sugihara (1999) coined it as the Laplace interpolant which is the name we choose to use here. We now define the Laplace shape function. Let $\mathbf{N}$ denote a nodal set which was defined previously, with V_I the Voronoi cell associated with node I. Let t_{IJ} be the $(d-1)$-dimensional facet (line segment in 2-d and polygon in 3-d) that is common to V_I and V_J, and $m(t_{IJ})$ denote the Lebesgue measure of t_{IJ}, i.e., a length in 2-d and an area in 3-d. If I and J do not have a common facet, then $m(t_{IJ}) = 0$. Now, consider the introduction of a point p with coordinate $\mathbf{x} \in \mathbf{R}^d$ into the tessellation. If the point p has n natural neighbors, then the Laplace shape function for node I is defined as [Christ, Friedberg, and Lee (1982); Belikov, Ivanov, Kontorovich, Korytnik, and Semenov (1997)]:

$$\phi_I(\mathbf{x}) = \frac{\alpha_I(\mathbf{x})}{\sum_{J=1}^{n} \alpha_J(\mathbf{x})}, \quad \alpha_J(\mathbf{x}) = \frac{m(t_J(\mathbf{x}))}{h_J(\mathbf{x})}, \quad \mathbf{x} \in \mathbf{R}^d. \tag{3}$$

In 2-d, the shape function takes the form:

$$\phi_I(\mathbf{x}) = \frac{\alpha_I(\mathbf{x})}{\sum_{J=1}^{n} \alpha_J(\mathbf{x})}, \quad \alpha_J(\mathbf{x}) = \frac{s_J(\mathbf{x})}{h_J(\mathbf{x})}, \quad \mathbf{x} \in \mathbf{R}^2, \tag{4}$$

where $\alpha_J(\mathbf{x})$ is the *Laplace weight function*, $s_I(\mathbf{x})$ is the length of the Voronoi edge associated with p and node I, and $h_I(\mathbf{x})$ is the Euclidean distance between p and node I (Fig. 2b).

The Voronoi diagram of the nodal set $\mathbf{N}$ defines the topology of a random lattice, such as those used to study breakdown processes in disordered materials [Herrmann

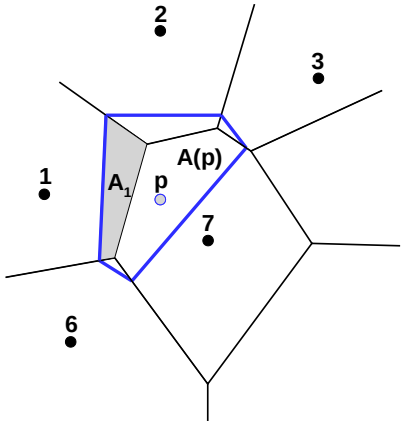

(a)

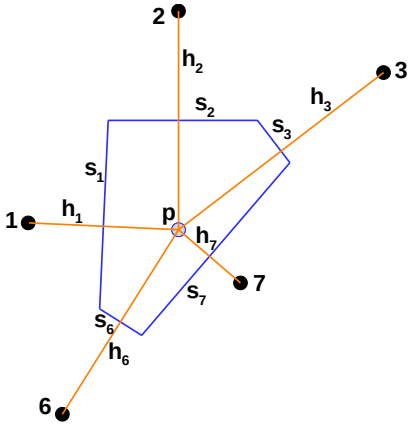

(b)

Figure 2 : Natural neighbor-based interpolants. (a) Sibson interpolant; and (b) Laplace interpolant.

and Roux (1990)]. The nodes act as lattice sites and are interconnected with their natural neighbors via simple lineal elements. For diffusion problems, the lattice elements can be viewed as conduits that transmit potential flow. Here, the quantity $\alpha_J = s_J/h_J$ in Equation (4) is used to scale the local diffusivity relations for the element connecting nodes I and J. The notion of a lattice network of conduit elements is discussed more fully in Section 3.2.2, which concerns the extraction of nodal gradient information based on the conservation of volume of the transmitted medium.

2.1 Properties

If the point $\mathbf{x} \to \mathbf{x}_I$, then $\phi_I(\mathbf{x}) = 1$ and all other shape functions are zero. The properties of positivity, interpolation, and partition of unity are true for the Sibson and the Laplace shape functions [Sukumar (1998); Sukumar, Moran, Semenov, and Belikov (2001)]:

$$0 \le \phi_I(\mathbf{x}) \le 1, \quad \phi_I(\mathbf{x}_J) = \delta_{IJ}, \quad \sum_{I=1}^{n} \phi_I(\mathbf{x}) = 1. \tag{5}$$

The Laplace shape functions also form a linearly complete approximation [Christ, Friedberg, and Lee (1982)]:

$$\mathbf{x} = \sum_{I=1}^{n} \phi_I(\mathbf{x})\mathbf{x}_I, \tag{6}$$

which indicates that the Laplace shape function can exactly reproduce a linear function. In a Galerkin implementation [Sukumar, Moran, Semenov, and Belikov (2001)], the Laplace interpolation scheme for a scalar-valued function $u(\mathbf{x})$ is written as:

$$u^h(\mathbf{x}) = \sum_{I=1}^{n} \phi_I(\mathbf{x})u_I, \tag{7}$$

where u_I ($I = 1, 2, \ldots, n$) are the unknowns at the n natural neighbors. On taking the derivative of Equation (7), we obtain:

$$\frac{\partial u^h}{\partial x_i}(\mathbf{x}) = \sum_{I=1}^{n} \phi_{I,i}(\mathbf{x})u_I \quad (i = 1\text{–}3). \tag{8}$$

2.2 Computational Algorithm

Simple geometric computations are required to compute the Lebesgue measure (s_{IJ}) that appears in the Laplace weight function. In 2-d, s_{IJ} is the Voronoi edge length, which is equal to the distance between adjacent Voronoi vertices. Algebraic formulas (see Sukumar (1998)) for the circumcenter of a triangle are used to evaluate the coordinate of the Voronoi vertices. For a triangle $t(A,B,C)$ with vertices $A(\mathbf{a})$, $B(\mathbf{b})$, and $C(\mathbf{c})$, the circumcenter (v_1, v_2) of t is:

$$v_1 = \frac{(a_1^2 - c_1^2 + a_2^2 - c_2^2)(b_2 - c_2)}{D} - \frac{(b_1^2 - c_1^2 + b_2^2 - c_2^2)(a_2 - c_2)}{D}, \tag{9a}$$

$$v_2 = \frac{(b_1^2 - c_1^2 + b_2^2 - c_2^2)(a_1 - c_1)}{D} - \frac{(a_1^2 - c_1^2 + a_2^2 - c_2^2)(b_1 - c_1)}{D}, \tag{9b}$$

where D which is four times the area of triangle $t(A,B,C)$ is given by

$$D = 2[(a_1 - c_1)(b_2 - c_2) - (b_1 - c_1)(a_2 - c_2)]. \quad (9c)$$

In Equation (9), $\mathbf{a} = (a_1, a_2)$, $\mathbf{b} = (b_1, b_2)$, and $\mathbf{c} = (c_1, c_2)$ are the coordinates of the vertices (oriented counter-clockwise) of t.

In 3-d, the Voronoi facet is a polygon, and the coordinates of the vertices are defined by the centers of the Delaunay circumspheres. The polygonal area is the Lebesgue measure s_{IJ}. From a sequential listing of the polygon vertices, the polygon area can be computed as follows. The polygonal domain is partitioned into a collection of triangles. The polygon area is then the sum of triangle areas, where the area of a triangle $t(A,B,C)$ in 3-d is given by

$$\Delta = \frac{\sqrt{E^2 + F^2 + G^2}}{2}, \quad (10)$$

where

$$\begin{aligned} E &= (b_2 - a_2)(c_3 - a_3) - (b_3 - a_3)(c_2 - a_2), \\ F &= (b_1 - a_1)(c_3 - a_3) - (b_3 - a_3)(c_1 - a_1), \\ G &= (b_1 - a_1)(c_2 - a_2) - (b_2 - a_2)(c_1 - a_1). \end{aligned} \quad (11)$$

Here, $\mathbf{a} = (a_1, a_2, a_3)$, $\mathbf{b} = (b_1, b_2, b_3)$, and $\mathbf{c} = (c_1, c_2, c_3)$ are the coordinates of the vertices of t in counter-clockwise order.

3 Discrete Differential Operators

First, we consider the approximation of the diffusion operator on unstructured grids and present numerical solutions for elliptic equations in 1-d and 3-d. Then, two different schemes for the extraction of the discrete nodal gradient are described, and numerical examples are presented to demonstrate the accuracy of the two schemes.

3.1 Difference Approximation for the Diffusion Operator

The Voronoi tessellation and its dual the Delaunay triangulation are often used to discretize a continuum. The Voronoi cell provides a natural domain of influence for a given node, and hence it is commonly used in numerical methods such as the finite volume and the finite element method. In the Voronoi cell finite element method (VCFEM) [Ghosh and Moorthy (1995)], the Voronoi tessellation is used to represent the material microstructure and a finite element formulation is developed on the Voronoi cells. The numerical method is used for multi-scale analysis of heterogeneous materials.

In this work, we use an integral balance law on the Voronoi cell (finite-volume averaging) to derive a finite difference scheme for the diffusion operator. The motivation for the above is derived from prior work on the Laplace interpolant [Belikov, Ivanov, Kontorovich, Korytnik, and Semenov (1997); Sukumar, Moran, Semenov, and Belikov (2001)] and from Friedberg and Ruiz (1984), in which prescriptions are presented for vector identities on a random lattice. The proposed approach was introduced in Sukumar (2003), but the authors recently became aware of the work of Börgers and Peskin (1985, 1987)], who have used the same scheme on Voronoi grids to approximate the Laplacian. In Börgers and Peskin (1985, 1987), the discrete Laplacian is used within a Lagrangian fractional step method for the solution of the Navier-Stokes equation. As our model problem, we consider the following d-dimensional steady-state diffusion equation with Dirichlet boundary conditions:

$$-Lu(\mathbf{x}) = -\boldsymbol{\nabla} \cdot \big(\kappa(\mathbf{x}) \boldsymbol{\nabla} u(\mathbf{x})\big) = f(\mathbf{x}) \quad \text{in } \Omega \quad (12a)$$

$$u(\mathbf{x}) = g(\mathbf{x}) \quad \text{on } \partial\Omega, \quad (12b)$$

where $\boldsymbol{\nabla}$ is the gradient operator, Ω is an open set in $\mathbf{R}^d$, and $\partial\Omega$ is the boundary of Ω. If $\kappa \equiv 1$, then L is the Laplacian operator. The model diffusion problem in Equation (12) is solved using a finite difference method, or equivalently a point collocation scheme [Aluru (2000)]. The discrete form of Equation (12) is:

$$-L_h u(\mathbf{x}_I) = f(\mathbf{x}_I), \quad I = 1, 2, \ldots, M \ (\mathbf{x}_I \in \Omega) \quad (13a)$$

$$u(\mathbf{x}_I) = g(\mathbf{x}_I) \quad \mathbf{x}_I \in \partial\Omega, \quad (13b)$$

where M is the number of the nodes in the domain, L_h is the discrete diffusion operator, and u_h is the finite difference approximation (h is a measure of the nodal spacing).

For ease of exposition, we focus on the 2-d case. Consider the domain Ω shown in Fig. 1c which is reproduced in Fig. 3a. The point p that was added to the tessellation is now assumed to denote a node. We can write the balance law for the divergence of the flux ($\mathbf{q} = -\kappa \boldsymbol{\nabla} u$) over the Voronoi cell A_I (see Fig. 3b) in the form:

$$-(Lu)_I = -\lim_{A_I \to 0} \frac{\int_{A_I} \boldsymbol{\nabla} \cdot \big(\kappa(\mathbf{x}) \boldsymbol{\nabla} u\big)\, d\Omega}{A_I}, \quad (14)$$

or

$$-(Lu)_I = -\lim_{A_I \to 0} \frac{\int_{\partial A_I} \kappa(\mathbf{x}) \dfrac{\partial u}{\partial n} d\Gamma}{A_I}, \tag{15}$$

where A_I is the area of the Voronoi cell of node I, and Gauss's (divergence) theorem has been invoked to convert the volume integral to a surface integral.

On using a cell-based central difference scheme for the normal derivative of u (see Fig. 3b), and the harmonic average [Narasimhan and Witherspoon (1976)] of the nodal diffusivities for the diffusive coefficient $\kappa(\mathbf{x})$, the above equation can be written as:

$$-(L_h u)_I = -\frac{1}{A_I} \sum_{J=1}^{n} \kappa_{IJ} \frac{(u_J - u_I)}{h_{IJ}} s_{IJ}, \tag{16a}$$

$$\frac{2}{\kappa_{IJ}} = \frac{1}{\kappa_I} + \frac{1}{\kappa_J}, \tag{16b}$$

where n is the number of natural neighbors for node I ($n = 5$ in Fig. 3b), h_{IJ} is the distance between nodes I and J, and s_{IJ} is the length of the Voronoi edge associated with nodes I and J (Fig. 3b). On using Equation (4) with $\kappa \equiv 1$ and after some algebraic simplification, the approximation for the negative Laplacian operator is [Börgers and Peskin (1985); Sukumar (2003)]:

$$-(L_h u)_I = -\frac{1}{A_I} \left[\left(\sum_{J=1}^{n} \alpha_{IJ} u_J \right) - \alpha_I u_I \right], \tag{17a}$$

$$\alpha_I = \sum_{J=1}^{n} \alpha_{IJ}, \quad A_I = \frac{1}{4} \sum_{J=1}^{n} s_{IJ} h_{IJ}, \tag{17b}$$

where $\alpha_{IJ} = s_{IJ}/h_{IJ}$ is the Laplace weight. The above expression is consistent with the prescription introduced for the discrete Laplacian on a random lattice [Friedberg and Ruiz (1984)]. The right-hand side of Equation (13a) is just f_I. Hence, the discrete system for the Poisson equation can be written as:

$$\begin{aligned} &\mathbf{K}\mathbf{u} = \tilde{\mathbf{f}}, \\ &\mathbf{K}_{II} = \alpha_I, \ \mathbf{K}_{IJ} = -\alpha_{IJ} (I \neq J), \ \ \mathbf{x}_I \in \Omega, \\ &\tilde{\mathbf{f}}_I = f_I A_I, \ \ \mathbf{x}_I \in \Omega, \\ &u_I = g(\mathbf{x}_I), \ \ \mathbf{x}_I \in \partial\Omega. \end{aligned} \tag{18}$$

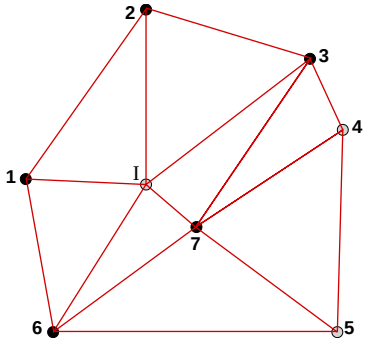

(a)

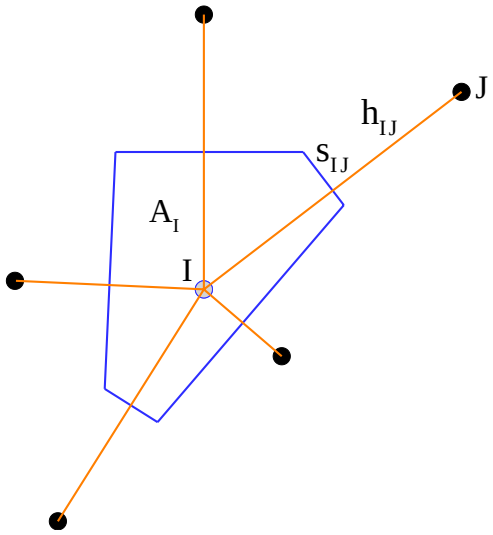

(b)

Figure 3 : Finite difference approximation at node I. (a) Node I in the triangulation; and (b) Voronoi cell of node I and its natural neighbors.

3.1.1 *Consistency and Convergence*

Consider the 1-d grid shown in Fig. 4. The stiffness matrix for the difference scheme is:

$$\mathbf{K}_{II} = \frac{1}{h_I} + \frac{1}{h_{I+1}}, \quad \mathbf{K}_{IJ} = -\frac{1}{h_I} \ (J = I - 1), \tag{19a}$$

$$\mathbf{K}_{IJ} = -\frac{1}{h_{I+1}} \ (J = I + 1), \tag{19b}$$

which is readily shown to be identical to that obtained using linear finite elements. In Börgers and Peskin (1985, 1987), the equivalence in 2-d is also shown. However, the right-hand side f is treated differently in both methods—

in finite elements, a weighted-integral value $\int_\Omega f N_I \, dV$ is assigned to the Ith row in the external force vector, whereas in the difference scheme, collocation at the node is used. Hence, the solution obtained by the two methods will in general be different (see Section 3.1.3).

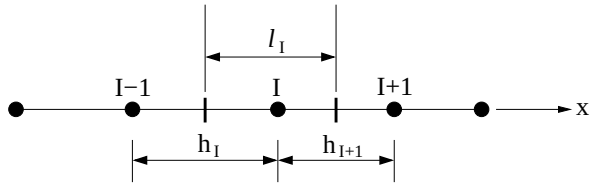

Figure 4 : Voronoi cell for a non-uniform grid in 1-d.

An interesting theoretical aspect is that of consistency on non-uniform grids, which has been extensively studied for cell- and vertex-centered difference schemes. Consistency in finite difference schemes ensures that in the limit when the grid spacing tends to zero, the difference between the finite difference scheme for the differential operator and the continuous form of the same is zero. We use the Taylor series expansion to study consistency in 1-d for the Laplace operator. Consider a direction n with unit vector $\mathbf{n} = (\pm 1, 0)$ in 1-d and let h be a scalar (grid-spacing). The Taylor series approximation for a function $u(x)$ at $\tilde{x} = x \pm h$ is written as:

$$u(x \pm h) = u(x) \pm u'(x)h + u''(x)\frac{h^2}{2} \pm u'''(x)\frac{h^3}{6} + O(h^4). \quad (20)$$

Now, on using the above Taylor series expansion at neighbors $I-1$ and $I+1$, we can write:

$$u_{I-1} = u_I - u'(x_I)h_I + u''(x_I)\frac{h_I^2}{2} - u'''(x_I)\frac{h_I^3}{6} + O(h_I^4), \quad (21a)$$

$$u_{I+1} = u_I + u'(x_I)h_{I+1} + u''(x_I)\frac{h_{I+1}^2}{2} + u'''(x_I)\frac{h_{I+1}^3}{6} + O(h_{I+1}^4). \quad (21b)$$

On multiplying both sides of Equations (21a) and (21b) by $1/h_I$ and $1/h_{I+1}$, respectively, and adding the result, we obtain

$$\frac{u_{I-1}}{h_I} + \frac{u_{I+1}}{h_{I+1}} = u_I\left(\frac{1}{h_I} + \frac{1}{h_{I+1}}\right) + u''(x_I)\left(\frac{h_I + h_{I+1}}{2}\right) + u'''(x_I)\frac{h_{I+1}^2 - h_I^2}{6} + O(h_{mI}^3), \quad (22)$$

where $h_{mI} = \max(h_I, h_{I+1})$. On using the definition of α_{IJ} and α_I that appear in Equation (17), and since $\ell_I = (h_I + h_{I+1})/2$, Equation (22) simplifies to

$$\frac{1}{\ell_I}\left[\sum_{J=1}^{2}\alpha_{IJ}u_J - \alpha_I u_I\right] = u''(x_I) + u'''(x_I)\left(\frac{h_{I+1} - h_I}{3}\right) + O(h_{mI}^2). \quad (23)$$

On using Equation (17) and noting that $Lu = u''(x_I)$ (Laplacian at node I), the above equation can be re-written as

$$Lu - L_h u = -u'''(x_I)\left(\frac{h_{I+1} - h_I}{3}\right) - O(h_{mI}^2) \quad (24)$$

and if $h_I \neq h_{I+1}$ (non-uniform grid), then

$$Lu - L_h u = -O(h_{mI}) \quad (25)$$

and hence in the limit that the grid spacing tends to zero, we have

$$\lim_{h_{mI} \to 0} Lu - L_h u = 0 \quad (26)$$

which shows that *first-order* consistency is obtained on non-uniform grids. If the nodal spacing is uniform (say h), then from Equation (24) we note that the coefficient of u''' also vanishes, and hence *second-order* consistency is established.

The traditional treatment of consistency and convergence via a Taylor series expansion on regular grids is not readily extendable to non-uniform grids. The notion of *flux consistency* appears to be important in the development of error estimates [Jones and Menzies (2000)] for difference schemes on Cartesian grids. Kreiss, Manteuffel, Swartz, Wendroff, and White, Jr. (1986) coined the term *supraconvergence* for schemes that converge at a higher-order than the local truncation error; supraconvergence has received a lot of attention in the numerical analysis literature for node- and cell-centered finite difference schemes. We point out that the *supraconvergence* phenomenon that is observed in finite-difference schemes on irregular grids is distinct from *superconvergence* in Galerkin finite element methods (see Wahlbin (1995)). In 2-d, the difference scheme is inconsistent (zeroth-order) on irregular grids, but second-order convergence in u is attained. A detailed theoretical analysis with supportive convergence tests is presented in Sukumar (2003).

3.1.2 Comparisons to Classical Finite Differences

Referring to the 1-d grid in Fig. 4 and on using Equation (17), the discrete approximation for the Laplacian ($Lu = u''$) at node I can be written as:

$$(L_h u)_I = \frac{2}{h_I + h_{I+1}} \left[\frac{1}{h_I} u_{I-1} + \frac{1}{h_{I+1}} u_{I+1} - \left(\frac{1}{h_I} + \frac{1}{h_{I+1}} \right) u_I \right]. \quad (27)$$

If $h_I = h_{I+1} = h$ (uniform grid), we obtain the classical central-difference approximation:

$$(L_h u)_I = \frac{u_{I-1} + u_{I+1} - 2u_I}{h^2}, \quad (28)$$

and if for example $h_I = 3\Delta x/4$, $h_{I+1} = 3\Delta x/2$, then

$$(L_h u)_I = \frac{16}{27\Delta x^2}(2u_{I-1} - 3u_I + u_{I+1}), \quad (29)$$

which is identical to the expression given in Thomas (1995), where cell-centered finite difference schemes are derived on non-uniform grids.

The Voronoi cell finite difference approximation for the Laplacian is identical to the classical finite difference scheme on rectangular and hexagonal grids in 2-d [Sukumar (2003)]. Here, we show the correspondence on a regular cubic lattice in 3-d. Consider a cubic lattice with nodal spacing h in the coordinate directions. We can write the finite difference approximation for the Laplacian at an interior node I as:

$$\nabla_h^2 u = \frac{1}{A_I} \left[\sum_{J=1}^{6} \alpha_{IJ} u_J - \alpha_I u_I \right], \quad (30)$$

where α_{IJ} is the Laplace weight, and node I has six neighbors (two in each coordinate direction). In this case, $A_I = h^3$, $s_{IJ} = h^2$, $h_{IJ} = h$, and since $\alpha_{IJ} = s_{IJ}/h_{IJ}$, we have $\alpha_{IJ} = h \; \forall J$. The above equation can be written as

$$\nabla_h^2 u = \frac{1}{h^3} \left[h\big(u_1 + u_2 + u_3 + u_4 + u_5 + u_6\big) - 6hu_I \right], \quad (31)$$

and hence

$$\nabla_h^2 u = \frac{u_1 + u_2 + u_3 + u_4 + u_5 + u_6 - 6u_I}{h^2} \quad (32)$$

which is the six-point finite difference stencil for the Laplacian on a regular grid in 3-d.

3.1.3 Numerical Examples

We explore the application of the difference scheme to the Poisson equation in 1-d and 3-d; in Sukumar (2003), numerical solutions in 2-d are presented. In 1-d, we consider the following Dirichlet boundary-value problem:

$$-u'' = \pi^2 \sin(\pi x) \quad \text{in } \Omega = (0,1), \quad (33a)$$

$$u(0) = u(1) = 0, \quad (33b)$$

with the exact solution $u(x) = \sin(\pi x)$. In our analysis, the L^∞ (max or sup) discrete error norm is defined as:

$$\|u - u_h\|_{\infty,\Omega} = \max_{I=1,\ldots,M} |u(x_I) - u_h(x_I)|, \quad (34)$$

where u and u_h are the exact and the finite difference solutions, respectively. In addition, the L^∞ discrete norm for the truncation error is given by

$$\|\tau\|_{\infty,\Omega} = \max_{I=2,\ldots,M-1} |\tau_I|, \quad (35a)$$

where

$$\tau_I = -\frac{1}{h_I} u(x_{I-1}) + \left(\frac{1}{h_I} + \frac{1}{h_{I+1}} \right) u(x_I) - \frac{1}{h_{I+1}} u(x_{I+1}) - \pi^2 \sin(\pi x_I) \quad (35b)$$

is the truncation error at node I for Equation (33a). In the above equations, $u(\cdot)$ is the nodal value of the exact solution, and the definitions for h_I and h_{I+1} are shown in Fig. 4. The sup-norms are evaluated for different maximum cell size $\ell_m = \max_I \ell_I$, where $\ell_I = (h_I + h_{I+1})/2$, and the rate of convergence is estimated by the slope on a log-log plot.

We considered non-uniform grids in 1-d to test the order of convergence of the truncation error and also of u. Since the grids chosen are random with inherent variability in the grid size, these rates of convergence are to be viewed in an average-sense, as opposed to precise estimates that are obtained with uniform refinement. A similar approach to compute the convergence rate was adopted by Jones and Menzies (2000) for the cell-centered finite volume method. A uniform random number between 20 and 200 was chosen to be the grid size (number of nodes M). Then, the spatial coordinate of the M nodes was set by picking $M-2$ random numbers between zero and unity (two nodes were assigned

the coordinates $x = 0$ and $x = 1$). To conduct the convergence study on non-uniform grids, we executed 1000 independent simulations. In Fig. 5, the results for the Poisson problem are presented. From Fig. 5a, it is observed that the truncation error decreases as $O(h)$, whereas in Fig. 5b, the error in u behaves as $O(h^2)$. The method displays the property of *supraconvergence* [Kreiss, Manteuffel, Swartz, Wendroff, and White, Jr. (1986); Jones and Menzies (2000)], i.e., the solution error decreases at a faster rate than is implied by the truncation error. Comparisons of the finite-difference, finite element, and the exact solution on a random grid of 25 nodes are shown in Fig. 5c.

To study the application of the finite difference scheme in 3-d, we consider the following Dirichlet boundary-value problem:

$$\nabla^2 u = 0 \quad \text{in } \Omega = (-1,1)^3 \tag{36a}$$

$$u = xy + yz + xz \quad \text{on } \partial\Omega, \tag{36b}$$

with the exact solution: $u = xy + yz + xz$. In the 3-d computations, nodes are first placed on each face of the bi-unit cube to facilitate the specification of boundary conditions. Thereafter, nodes are randomly positioned within the interior of the bi-unit cube using a pseudo-random number generator. Four grids are considered to test the convergence: 242 nodes, 542 nodes, 1593 nodes, and 3568 nodes, with mean nodal spacing $h = 0.42, 0.32, 0.21, 0.16$, respectively. The nodal grids with 242 and 3568 nodes are shown in Figures 6a and 6b, respectively. In our analysis, the L^2 discrete error norm is defined as:

$$\|u - u_h\|_{2,\Omega} = \left(\sum_{I=1}^{M} A_I \big(u(\mathbf{x}_I) - u_h(\mathbf{x}_I) \big)^2 \right)^{1/2}. \tag{37}$$

The relative error in the L^2 norm is plotted in Fig. 6c, where the slope λ is the rate of convergence. The convergence rate is computed using a mean grid size for the measure h; second-order accuracy is observed.

3.2 Difference Approximation for the Gradient Operator

We discuss the extraction of nodal gradients of a scalar (potential) field. The Voronoi cell can be used to define a local discrete gradient operator. A non-local smoothing procedure (finite volume averaging) renders the following approximation for the nodal gradient operator [Chen,

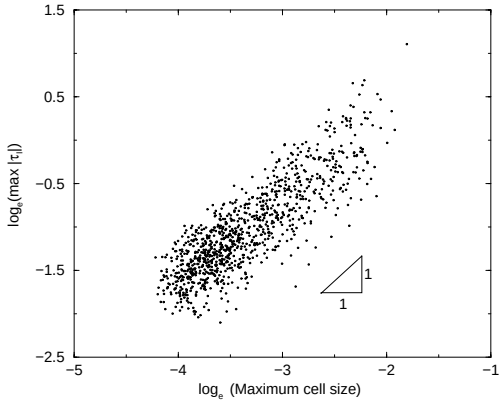

(a)

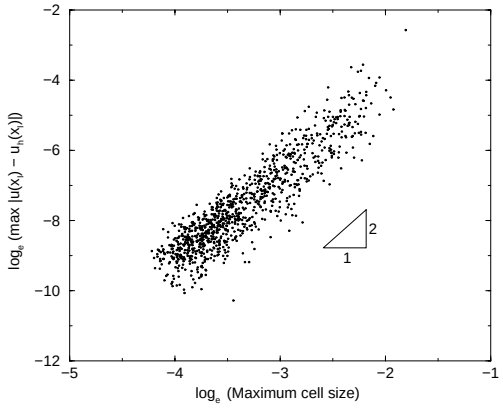

(b)

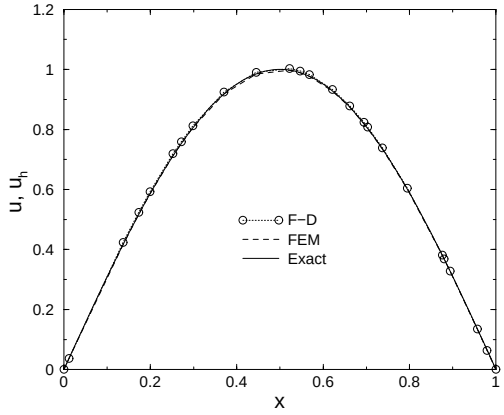

(c)

Figure 5 : Poisson problem in 1-d. (a) Convergence of truncation error; (b) Convergence of solution error; and (c) Comparison of numerical and exact solutions.

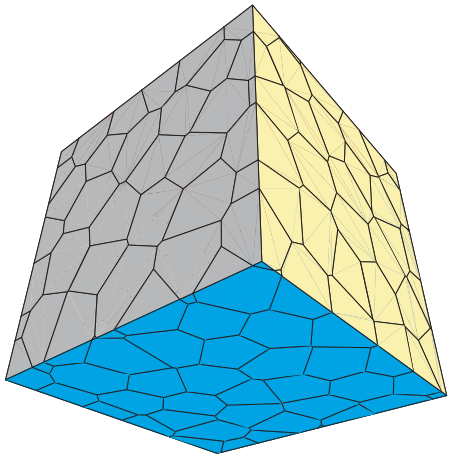

(a)

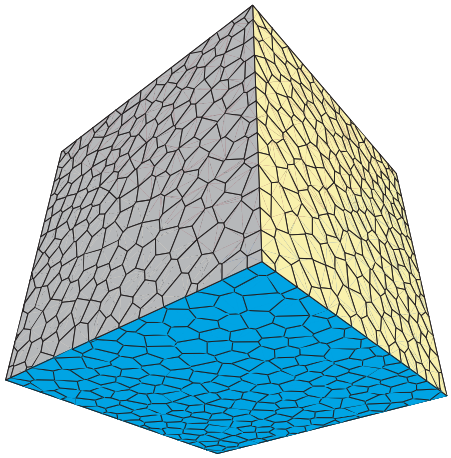

(b)

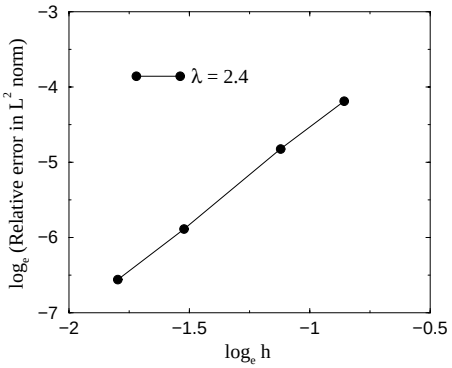

(c)

Figure 6 : Laplace problem in 3-d. (a) Grid (242 nodes); (b) Grid (3568 nodes); and (c) Convergence.

Wu, Yoon, and You (2001)]:

$$\frac{\partial u^h}{\partial x_j}(\mathbf{x}_I) = \frac{\int_{A_I} u^h_{,j}(\mathbf{x})\, d\Omega}{A_I} = \frac{\int_{\partial A_I} u^h(\mathbf{x}) n_j\, d\Gamma}{A_I}, \qquad (38)$$

where Gauss's divergence theorem has been invoked. In Chen, Wu, Yoon, and You (2001), numerical quadrature was used to compute the above surface integral. In this paper, we adopt the Voronoi cell and the notion of natural neighbors, to propose two approaches to compute the nodal gradient. In the first scheme, the derivative of the Laplace interpolant is used as a weighting function, whereas the second method is based on volume conservation in fluid flow, or equivalently force equilibrium in elasticity.

3.2.1 Nodal Gradient Based on the Laplace Interpolant

In a Galerkin method, the natural neighbor-based interpolation scheme in Equation (7) is used to evaluate $u^h(\mathbf{x})$ at any point within the domain Ω. In moving to a finite-difference setting, we can reconstruct the same picture by imagining that a node located at $\mathbf{x}_I$ has been removed and subsequently re-inserted at the same location ($\mathbf{x} = \mathbf{x}_I$) in the grid (see Fig. 3a). The means to define the approximation at a point p (continuum perspective) vis-à-vis that at a node (lattice perspective) is noted. This viewpoint extends to the evaluation of the discrete nodal gradient, too. The gradient at node I is evaluated by assuming that node I is inserted into the tessellation and a discrete approximation for $u_{,j}$ at $\mathbf{x}_I$ ($\mathbf{x} \equiv \mathbf{x}_I$) is computed. Referring to Equation (8), we can approximate the gradient of a scalar-valued function u at $\mathbf{x}_I$ as:

$$(\boldsymbol{\nabla} u)_I = \frac{\partial u_h}{\partial x_i}\mathbf{e}_i = \sum_{J=1}^{n} w^i_{IJ}(\mathbf{x}_I) u_J \mathbf{e}_i \equiv \sum_{J=1}^{n} \phi_{J,i}(\mathbf{x}_I) u_J \mathbf{e}_i, \qquad (39)$$

where $n = 5$ for node I in Fig. 3, $\mathbf{e}_i$ are the Cartesian unit base vectors (sum on i is implied in the above equation), and the weight $w^i_{IJ}(\mathbf{x}_I)$ is the derivative of the Laplace shape function in the x_i-coordinate direction.

3.2.2 Conservative Scheme for the Evaluation of Nodal Gradients

The discrete modeling of the Laplace equation can be accomplished by using a random lattice of lineal conduit elements, where the generator points (nodes) of the Voronoi cells act as the lattice sites and the conduit elements provide flow paths between natural neighbors. We

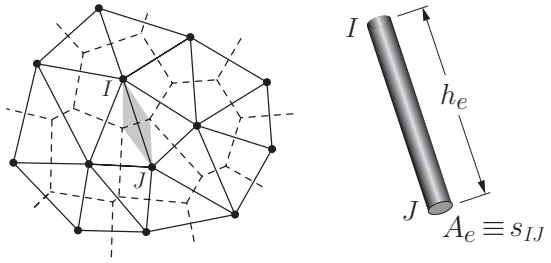

Figure 7 : Conduit network and scaling relation.

set the cross-section area of an element connecting natural neighbors I and J equal to the Voronoi facet area s_{IJ} that is common to both neighbors. For a two-dimensional lattice, the element contribution to the network equilibrium equations is:

$$\mathbf{K}_e = \frac{\kappa_{IJ} A_{IJ}}{h_{IJ}} \begin{bmatrix} 1 & -1 \\ -1 & 1 \end{bmatrix} \equiv \frac{\kappa_{IJ} s_{IJ}}{h_{IJ}} \begin{bmatrix} 1 & -1 \\ -1 & 1 \end{bmatrix}, \quad (40)$$

where κ_{IJ} is the diffusivity of the element. These local diffusivity relations have the same form as that of two-node finite elements used for analyzing potential flow problems (Fig. 7). The direct stiffness approach is used to assemble elemental contributions into global network equations of the form $\mathbf{Ku} = \mathbf{f}$. The key point, which is shown through the examples that follow, is the use of the s_{IJ}/h_{IJ} scaling within the elemental relations.

In Fig. 8, two Voronoi discretizations of a homogeneous medium ($l \times l$ square domain) are shown. Potential is prescribed on the left- and right-hand sides of the domain, whereas the top and bottom surfaces are assumed to be perfect insulators. With no loss of generality, the diffusion coefficient κ is set equal to unity. For a potential difference of magnitude l acting across the domain, theory predicts a steady state potential $u = x$ in the domain. From the error norm results presented in Tab. 1, it is observed that the random lattice approach captures the linear potential field to within machine precision. The numerical results also demonstrate that this approach does not exhibit spurious heterogeneity arising from either random mesh geometry or varying nodal spacing. As a matter of comparison, the error norms arising from the use of a constant area A_{IJ} in Equation (40) are also presented in Tab. 1. In essence, s_{IJ} in Equation (40) has been replaced by the average of s_{IJ} for the whole domain. It is observed that on using a constant area measure, a linear potential field (patch test) can not be exactly represented on a lattice.

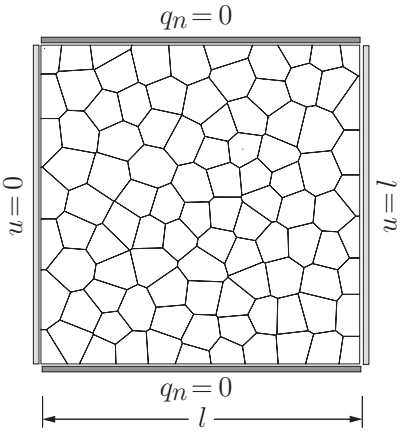

(a)

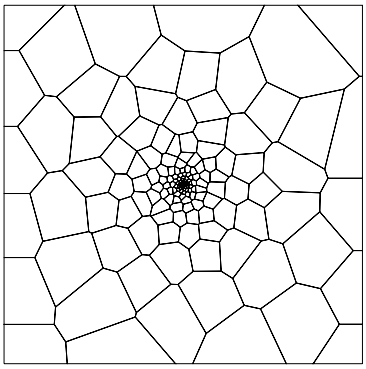

(b)

Figure 8 : Voronoi diagram for grids used in the extraction of nodal gradients. (a) Quasi-uniform grid; (b) Graded grid.

After solving for the vector of nodal potentials **u**, as outlined above, the flow Q_{IJ} between nodes I and J can be related to the potential difference between the two nodes:

$$Q_{IJ} = \frac{\kappa_{IJ} s_{IJ}}{h_{IJ}} (u_J - u_I). \quad (41)$$

Since the geometry of the network bears no relation to any material features, the flow in the conduit elements themselves has little practical meaning. However, gradient information at node I can be computed from the elemental flow values as follows. With reference to the two-dimensional case illustrated in Fig. 9, the procedure to extract the nodal flux (gradients) is described below:

Table 1 : Error in the L^2- and L^∞-norms for the potential problem.

Grid	$A_{IJ} = s_{IJ}/h_{IJ}$		Constant A_{IJ}	
	$\|u-u_h\|_2$	$\|u-u_h\|_\infty$	$\|u-u_h\|_2$	$\|u-u_h\|$
Fig. 8a	3.9×10^{-15}	1.5×10^{-15}	2.1×10^{-1}	$4.3\times10^{-}$
Fig. 8b	1.5×10^{-14}	2.6×10^{-15}	5.0×10^{-1}	$9.0\times10^{-}$

- section the associated Voronoi cell through its node I with a cut plane with inclination ψ.
- determine the weighting factor R_J applied to flow through each facet of the cell. There are three possible cases for a given face that is associated with node J:
  1. $R_J = 1$ when both facet vertices are on the positive (i.e., shaded) side of the cut plane;
  2. $R_J = 0$ when both facet vertices are on the negative side of the cut plane;
  3. $0 < R_J = a_J/s_{IJ} < 1$ when facet vertices appear on both sides of the cut plane. Here, a_J is the facet length on the positive side of the cut plane and s_{IJ} is the length of the Voronoi edge associated with nodes I and J.
- compute the net flow Q^I_ψ through the cut face by summing the weighted flow values for each face (i.e., for each conduit element framing into the node):

$$Q^I_\psi = \sum_{J=1}^{n} R_J Q_{IJ}, \tag{42}$$

  where n is the total number of facets of the Voronoi cell. In Fig. 9, the flows Q_{IJ} are indicated by solid lines on Voronoi edges that contribute and by dotted lines on edges that do not contribute in the above summation.
- determine the nodal flux by dividing the net flow through the cut face by its area, A_ψ:

$$q^I_\psi = \frac{Q^I_\psi}{A_\psi}, \tag{43}$$

  where A_ψ is the distance between points m and n in Fig. 9.

This series of calculations can be repeated for any angle ψ to determine the potential gradient in the direction normal to the cut plane.

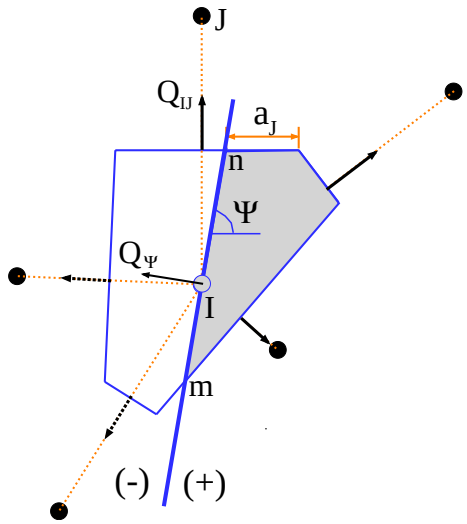

Figure 9 : Numerical scheme for extraction of nodal flux.

3.2.3 Numerical Results

In Tables 2 and 3, the numerical results for the nodal gradient computed by Scheme I (Section 3.2.1) and Scheme II (Section 3.2.2), respectively, are presented. The error in the L^∞ norm that is defined in Equation (34) is used to assess the accuracy of the schemes. The potential problem with $u = x$ as the exact solution is considered, and hence $\partial u/\partial x = 1$ and $\partial u/\partial y = 0$. For the conservative scheme, the nodal gradients have been determined for three cut plane inclinations: $\psi = 0$, $-\pi/4$, and $-\pi/2$, which correspond to $\partial u/\partial y$, $\partial u/\partial n$, and $\partial u/\partial x$, respectively. The numerical results obtained for both the schemes are exact to within machine precision.

Table 2 : Error in the L^∞ norm for the recovery of the nodal flux (Scheme I).

Grid	$\|u_{,x} - u_{h,x}\|_\infty$	$\|u_{,y} - u_{h,y}\|_\infty$
Fig. 8a	6.5×10^{-15}	5.3×10^{-15}
Fig. 8b	1.4×10^{-13}	1.3×10^{-13}

To demonstrate the accuracy of the conservative scheme for non-uniform flow problems, an impermeable inclusion is inserted into the center of the domain shown in

Table 3 : Error in the L^∞ norm for the recovery of the nodal flux (Scheme II).

Grid	$\|u_{,x} - u_{h,x}\|_\infty$	$\|u_{,y} - u_{h,y}\|_\infty$	$\|u_{,n} - u_{h,n}\|_\infty$
Fig. 8a	1.7×10^{-14}	1.0×10^{-14}	1.3×10^{-14}
Fig. 8b	3.1×10^{-13}	4.9×10^{-13}	4.7×10^{-13}

Fig. 8. The mesh and boundary conditions are shown in Fig. 10a. The inclusion radius a is small relative to the domain size (i.e., $a = l/100$), so that comparisons can be made to the theoretical solution for an infinite domain [Kirchhoff (1985)]:

$$\cos 2\theta = \frac{\left(\frac{a}{r}\right)^4 + 1 - q^2}{2\left(\frac{a}{r}\right)^2}, \qquad (44)$$

where (r, θ) are polar coordinates with the origin at the inclusion center, and q represents the flow rate. The accuracy of the model is demonstrated by comparing the numerical and theoretical results for the flow rate (Fig. 10b). The contour lines produced from the numerical model are in good agreement with the theoretical solution. The use of significantly coarser discretizations does provide reasonably accurate results, although the flow rate curves are not as smooth and the curves closest to the inclusion are not fully captured.

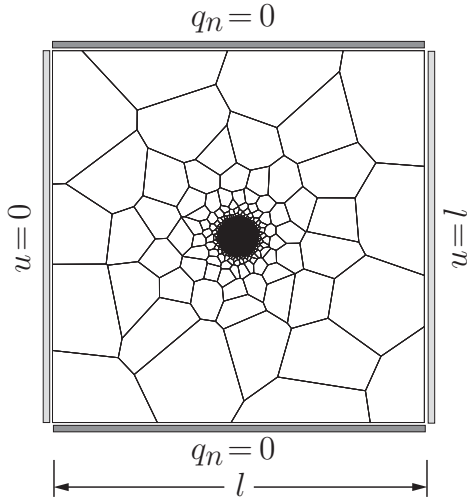

(a)

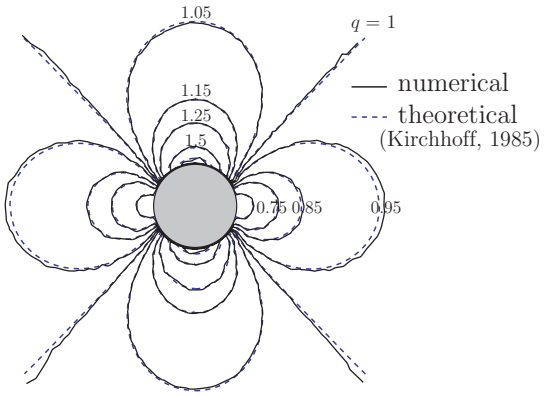

(b)

Figure 10 : Potential flow past cylindrical inclusion. (a) Mesh; and (b) Isocontours of flow rate q

4 Conclusions

Finite difference approximations for differential operators (diffusion and gradient) on non-uniform grids were presented. The diffusion operator at a node was approximated by its average integral-value over the Voronoi cell of the node. The Laplace weight measure naturally emerged in the difference approximation. The Laplace weight has also been in a Galerkin formulation [Sukumar, Moran, Semenov, and Belikov (2001)], as a scaling parameter in fracture simulations on rigid-body spring-networks [Bolander, Jr and Saito (1998)], and as a weight measure for random walk on arbitrary sets [Harris, Williams, and Sibson (1999)].

The Voronoi cell-based finite difference scheme was shown to reduce to the classical finite difference scheme on regular grids. Simple algebraic computations are only involved in determining the finite difference weights in 2-d as well as 3-d, and numerical examples were presented to demonstrate the accuracy of the method. Different schemes to compute the discrete nodal gradient on a non-uniform grid were discussed and applied to potential flow problems. The nodal gradient recovery was exact for a linear field, and accurate numerical solutions were also obtained for a non-linear potential field. Over the past decade, most of the developments on meshless methods have been within the framework of a Galerkin implementation. This study provides a link of a meshless interpolant to discrete differential operators on arbitrary unstructured grids.

Acknowledgement: The research support of the National Science Foundation through contract CMS–0201590 to the University of California, Davis, is gratefully acknowledged.

References

Aluru, N. R. (2000): A point collocation method based on reproducing kernel approximations. *International Journal for Numerical Methods in Engineering*, vol. 47, pp. 1083–1121.

Arroyo, M. (2003): Private communication.

Atluri, S. N.; Shen, S. (2002): *The Meshless Local Petrov-Galerkin (MLPG) Method*. Tech Science Press, Encino, CA.

Atluri, S. N.; Shen, S. (2002): The meshless local Petrov-Galerkin (MLPG) method: A simple & less-costly alternative to the finite element and boundary element methods. *CMES:Computer Modeling in Engineering & Sciences*, vol. 3, no. 1, pp. 11–52.

Aurenhammer, F. (1996): Voronoi diagrams — a survey of a fundamental geometric data structure. *ACM Transactions on Mathematical Software*, vol. 23, pp. 469–483.

Baty, R. S.; Villon, W. P. (1997): Least-squares solutions of a general numerical method for arbitrary irregular grids. *International Journal for Numerical Methods in Engineering*, vol. 140, pp. 1701–1717.

Belikov, V. V.; Ivanov, V. D.; Kontorovich, V. K.; Korytnik, S. A.; Semenov, A. Y. (1997): The non-Sibsonian interpolation: A new method of interpolation of the values of a function on an arbitrary set of points. *Computational Mathematics and Mathematical Physics*, vol. 37, no. 1, pp. 9–15.

Belytschko, T.; Krongauz, Y.; Organ, D.; Fleming, M.; Krysl, P. (1996): Meshless methods: An overview and recent developments. *Computer Methods in Applied Mechanics and Engineering*, vol. 139, pp. 3–47.

Bolander, Jr, J. E.; Saito, S. (1998): Fracture analyses using spring networks with random geometry. *Engineering Fracture Mechanics*, vol. 61, pp. 569–591.

Börgers, C.; Peskin, C. S. (1985): A Lagrangian method based on the Voronoi diagram for the incompressible Navier-Stokes equations on a periodic domain. In Fritts, M. J.; Crowley, W. P.; Trease, H.(Eds): *The Free Lagrange Method (Lecture Notes in Physics)*, volume 238, pp. 87–113, New York, N.Y. Springer-Verlag.

Börgers, C.; Peskin, C. S. (1987): A Lagrangian fractional step method for the incompressible Navier-Stokes equations on a periodic domain. *Journal of Computational Physics*, vol. 70, no. 2, pp. 397–438.

Breitkopf, P.; Touzot, G.; Villon, P. (2000): Double grid diffuse collocation method. *Computational Mechanics*, vol. 25, no. 2/3, pp. 199–206.

Chen, J. S.; Wu, C. T.; Yoon, S.; You, Y. (2001): A stabilized conforming nodal integration for Galerkin meshfree methods. *International Journal for Numerical Methods in Engineering*, vol. 50, pp. 435–466.

Christ, N. H.; Friedberg, R.; Lee, T. D. (1982): Weights of links and plaquettes in a random lattice. *Nuclear Physics B*, vol. 210, no. 3, pp. 337–346.

Cosmi, F. (2001): Numerical solution of plane elasticity problems with the cell method. *CMES:Computer Modeling in Engineering & Sciences*, vol. 2, no. 3, pp. 365–372.

Cueto, E.; Sukumar, N.; Calvo, B.; Cegoñino, J.; Doblaré, M. (2003): Overview and recent advances in natural neighbor Galerkin methods. *Archives of Computational Methods in Engineering*. in press.

Ferretti, E. (2003): Crack propagation modeling by remeshing using the cell method (CM). *CMES:Computer Modeling in Engineering & Sciences*, vol. 4, no. 1, pp. 51–72.

Friedberg, R.; Ruiz, M. (1984): Vector algebra on a lattice. *Physical Review D*, vol. 29, no. 12, pp. 2916–2918.

Ghosh, S.; Moorthy, S. (1995): Elastic-plastic analysis of arbitrary heterogeneous materials with the Voronoi cell finite-element method. *Computer Methods in Applied Mechanics and Engineering*, vol. 121, no. 1–4, pp. 373–409.

Harris, S. C.; Williams, D.; Sibson, R. (1999): Scaling random walks on arbitrary sets. *Mathematical Proceedings of the Cambridge Philosophical Society*, vol. 125, no. 3, pp. 535–544.

Herrmann, H. J.; Roux, S.(Eds): *Statistical Models for the Fracture of Disordered Media*. North-Holland, Amsterdam, The Netherlands.

Hiptmair, R. (2001): Discrete Hodge operators. *Numerische Mathematik*, vol. 90, no. 2, pp. 265–289.

Hirani, A. N. (2003): *Discrete Exterior Calculus*. Ph.D. thesis, California Institute of Technology, Pasadena, CA, U.S.A., 2003.

Hiyoshi, H.; Sugihara, K. (1999): Two generalizations of an interpolant based on Voronoi diagrams. *International Journal of Shape Modeling*, vol. 5, no. 2, pp. 219–231.

Hyman, J. M.; Shashkov, M. (1997): Natural discretization for the divergence, gradient, and curl on logically rectangular grids. *Computers & Mathematics with Applications*, vol. 33, no. 4, pp. 81–104.

Jensen, P. S. (1972): Finite difference techniques for variable grids. *Computers and Structures*, vol. 2, pp. 17–29.

Jones, W. P.; Menzies, K. R. (2000): Analysis of the cell-centred finite volume method for the diffusion equation. *Journal of Computational Physics*, vol. 165, pp. 45–68.

Kirchhoff, R. (1985): *Potential Flows: Computer Graphic Solutions*. Marcel Dekker, New York, N.Y.

Kreiss, H.; Manteuffel, T. A.; Swartz, B.; Wendroff, B.; White, Jr., A. B. (1986): Supra-convergent schemes on irregular grids. *Mathematics of Computation*, vol. 47, no. 176, pp. 537–554.

Lancaster, P.; Salkauskas, K. (1981): Surfaces generated by moving least squares methods. *Mathematics of Computation*, vol. 37, pp. 141–158.

Li, S.; Liu, W. K. (2002): Meshfree and particle methods and their applications. *Applied Mechanics Review*, vol. 55, no. 1, pp. 1–34.

Liszka, T.; Orkisz, J. (1980): The finite difference method at arbitrary irregular grids and its application in applied mechanics. *Computers and Structures*, vol. 11, pp. 83–95.

Mathieu, D.; Hirani, A. N.; Leok, M.; Marsden, J. E. (2003): Discrete exterior calculus. in preparation.

Narasimhan, T. N.; Witherspoon, P. A. (1976): An integrated finite difference method for analyzing fluid flow in porous media. *Water Resources Research*, vol. 12, no. 1, pp. 57–64.

Sibson, R. (1980): A vector identity for the Dirichlet tesselation. *Mathematical Proceedings of the Cambridge Philosophical Society*, vol. 87, pp. 151–155.

Sukumar, N. (1998): *The Natural Element Method in Solid Mechanics*. Ph.D. thesis, Theoretical and Applied Mechanics, Northwestern University, Evanston, IL, U.S.A., 1998.

Sukumar, N. (2003): Voronoi cell finite difference method for the diffusion operator on arbitrary unstructured grids. *International Journal for Numerical Methods in Engineering*, vol. 57, no. 1, pp. 1–34.

Sukumar, N.; Moran, B.; Semenov, A. Y.; Belikov, V. V. (2001): Natural neighbor Galerkin methods. *International Journal for Numerical Methods in Engineering*, vol. 50, no. 1, pp. 1–27.

Teixeira, F. L.; Chew, W. C. (1999): Lattice electromagnetic theory from a topological viewpoint. *Journal of Mathematical Physics*, vol. 40, no. 1, pp. 169–187.

Thomas, J. W. (1995): *Numerical Partial Differential Equations: Finite Difference Methods*. Springer-Verlag, New York.

Tonti, E. (2001): A direct discrete formulation of field laws: The cell method. *CMES:Computer Modeling in Engineering & Sciences*, vol. 2, no. 2, pp. 237–258.

Wahlbin, L. B. (1995): *Superconvergence in Galerkin Finite Element Methods*, volume 1605. Springer-Verlag, New York.

Warnick, K. F.; Selfridge, R. H.; Arnold, D. V. (1997): Teaching electromagnetic field theory using differential forms. *IEEE Transactions on Education*, vol. 40, no. 1, pp. 53–68.